Impacts of Sun Glint Off Ice Clouds on DSCOVR EPIC Cloud Products

Tamás Várnai, Alexander Marshak, Alexander B. Kostinski, Yuekui Yang, and Yaping Zhou

***Abstract*— The Earth Polychromatic Camera (EPIC) onboard the Deep Space Climate Observatory (DSCOVR) spacecraft observes the sunlit face of the Earth from a distance of about one-and-a-half million kilometers. Several studies demonstrated that EPIC images often feature sun glint from water surfaces and from horizontally oriented ice crystals occurring inside clouds. This study presents a statistical analysis of a yearlong EPIC dataset to gain insights into sun glints and their impacts on satellite measurements of cloudiness and cloud properties. The first results discussed demonstrate that over land, the observed glints, indeed, come mainly from ice clouds and not from small water bodies. Subsequent results reveal that sun glints affecting EPIC observations (especially at 388 nm) greatly increase the likelihood and sensitivity of cloud detection, particularly of the elusive thin and small ice clouds. Finally, the results indicate that sun glints often cause spurious increases in the cloud optical thickness (COT) and altitude values in the operational EPIC cloud product. Insights into the frequency, magnitude, and causes of glint effects and suggestions for future work are also provided.**

***Index Terms*— Atmosphere, clouds, ice, remote sensing.**

I. Introduction

THE Earth Polychromatic Camera (EPIC) onboard the Deep Space Climate Observatory (DSCOVR) spacecraft observes the Earth from a distance of about one-and-a-half million kilometers—that is, from a location about four times farther than the Moon [1]. EPIC always observes the sunlit face of our planet because DSCOVR orbits the Sun at the L1 Lagrangian point, which is near the straight line connecting the Sun and Earth. Typically, EPIC takes 22 images a day from late April to early September, and 13 images a day during the rest of the year [when DSCOVR can transmit less data as the ground communication station located at NASA's Wallops Flight Facility (Virginia), USA is visible from DSCOVR for shorter times during the shorter days]. EPIC uses a filter wheel to take images at ten wavelengths ranging from 317 to 780 nm. The spatial resolution is around 8 km at the image center and decreases toward the edge of the Earth disk.

The EPIC team provides a wide range of operational data products that are publicly available through the Atmospheric Science Data Center (ASDC) of the NASA Langley Research Center (https://search.earthdata.nasa.gov/). These products include calibrated and geolocated reflectances, as well as geophysical products ranging from land and ocean surface characteristics to the properties of atmospheric gases, aerosols, and clouds [1]. Recently, the suite of products was expanded by the release of the EPIC sun glint product [2].

A key part of this new product is the glint mask, which identifies EPIC pixels affected by sun glint—the specular reflection of sunlight—off smooth water surfaces and horizontally oriented ice crystals occurring in clouds. (The current glint product does not seek to identify glints off rough water surfaces.) The glint detection algorithm identifies such glints in the vicinity of the specular spot, which is the single location in each image where the EPIC view direction exactly matches the direction of specular reflection from a horizontal surface. While the EPIC view direction is constant all around this spot, the direction of specular reflection from horizontal surfaces changes with location due to the sphericity of Earth. The analysis of EPIC images found that glint effects from ice clouds and smooth water surfaces are significant as long as the glint angle—the angle between the EPIC view direction and the direction of specular reflection from a horizontal surface—remains below about 1.5° [3]. In practice, this means that glints are significant up to about ten pixels away from the specular spot [4].

Over the years, several studies analyzed such glints, examining characteristics, such as prevalence, size, and brightness, as well as spectral, geographical, and seasonal variations (see [5], [6], [7]). These studies followed in the footsteps of earlier studies that analyzed glint observations made by other satellite instruments such as the Polarization and Directionality of the Earth's Reflectance (POLDER) radiometer (see [8], [9], [10]) or the Cloud-Aerosol Lidar with Orthogonal Polarization (CALIOP) lidar (see [11], [12]). Several studies explored using glint off water surfaces to estimate the absorption properties of atmospheric aerosols (see [13], [14], [15]). Most studies, however, were motivated by gaining information about ice crystals that, instead of tumbling randomly through the air, maintain a stable horizontal orientation due to a balance of aerodynamic forces (see [8], [16]). The studies found that although horizontally oriented crystals represent a minority of all cloud particles, these crystals are often present in high

Manuscript received 9 August 2023; revised 13 January 2024 and 18 March 2024; accepted 6 April 2024. Date of publication 14 May 2024; date of current version 28 May 2024. This work was supported in part by the NASA DSCOVR Project and in part by the ACMAP Program. The work of Alexander B. Kostinski was supported in part by the National Science Foundation (NSF) under Grant AGS-2217182. *(Corresponding author: Tamás Várnai.)*

Tamás Várnai and Yaping Zhou are with the Goddard Earth Sciences Technology and Research (GESTAR) II, University of Maryland, Baltimore County, Baltimore, MD 21250 USA, and also with the NASA Goddard Space Flight Center, Greenbelt, MD 20771 USA (e-mail: varnai@umbc.edu; yaping.zhou@nasa.gov).

Alexander Marshak and Yuekui Yang are with the NASA Goddard Space Flight Center, Greenbelt, MD 20771 USA (e-mail: alexander.marshak@nasa.gov; yuekui.yang@nasa.gov).

Alexander B. Kostinski is with the Department of Physics, Michigan Technological University, Houghton, MI 49931 USA (e-mail: kostinsk@mtu.edu).

Digital Object Identifier 10.1109/TGRS.2024.3400253

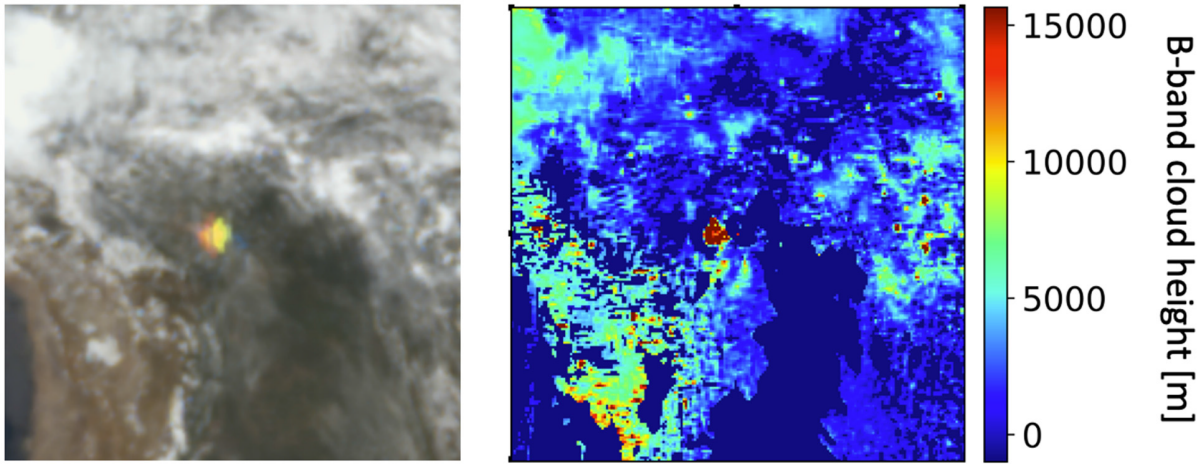

Fig. 1. Glints off ice clouds affect observed reflectances and apparent cloud heights retrieved from the reflectances. (Left) RGB image of a glint off ice clouds over Bolivia and (right) image of effective cloud height are approximately 200 × 200 pixels in size and show a scene observed by EPIC at around 16:30 UTC on February 13, 2017. The glint appears colorful in the RGB image because EPIC uses a filter wheel to take images at different wavelengths (https://epic.gsfc.nasa.gov/about/epic), which means that the image of each wavelength is taken at a slightly different time—and during the few minutes separating the images of various colors, the rotation of the Earth makes the glint appear at slightly different locations in the red, green, and blue images (there is a 4-min difference between blue (443 nm) and red (680 nm) images). The RGB image is from the EPIC website at epic.gsfc.nasa.gov; the effective cloud height (based on oxygen B-band data) is from the EPIC operational cloud product. A spurious increase in cloud height is observed over the glint region.

enough numbers for the direct reflection of sunlight from their horizontal top surfaces (which act like tiny mirrors) to create an observable glint—a phenomenon that is also called subsun in atmospheric optics (see [17], [18], [19]).

Understanding horizontally oriented particles (HOPs) is important because theoretical simulations show that HOPs and randomly oriented particles can result in very different cloud albedos and surface irradiances [20]; recently, this difference was shown to be quite significant in a long-term ground-based observational dataset [21]. HOPs also greatly influence polarization in instruments such as the global precipitation measurement (GPM) microwave imager (GMI) and can cause significant errors in microwave retrievals of cloud ice water path [22]. In addition, observing HOPs can provide information on ice cloud conditions such as particle shape, the level of turbulence, the likely presence of upward air motion, and even on the significance of radiative cooling in crystal growth [23]. Furthermore, horizontal orientation has a strong influence on the fall speed of ice crystals and hence on the lifetime of ice clouds (see [23], [24], [25]).

To help better understand HOPs, recent theoretical calculations provided detailed information on the radiative (single scattering) properties of HOPs (see [26], [27]), which can be of great help in interpreting sun glint observations or even lidar measurements [28], [29], [30], [31].

While glint observations offer excellent opportunities to gain new information, glints can also pose challenges in satellite retrievals of atmospheric and surface properties (see [32]). For example, to avoid errors caused by glints off water surfaces, the dark target aerosol product of the Moderate Resolution Imaging Spectroradiometer (MODIS) does not report aerosol properties over the ocean, whenever the glint angle is less than 40° (see [33], [34]). This is because even relatively faint, diffuse glint from rough water surfaces could bias the aerosol retrievals, which cannot accurately account for the glint due to its variations with wind and ocean current conditions.

Recently, the EPIC cloud team developed a technique to mitigate the impact of glints off ocean surfaces in retrievals of cloud properties [35]. Even more recently, new techniques were developed to improve the cloud detection and cloud property retrievals of the Himawari-8 satellite in regions, where sun glint can potentially affect the observations [36], [37]. Again, while the large area of surface glint (from glint center to 30°–40° glint angle) due to rough ocean is considered in these studies, the specular glints from ice crystals have not been considered. However, visual inspection of a few EPIC images suggested that glints off ice crystals impact retrieved cloud properties (Fig. 1). This article explores this impact by statistically analyzing a yearlong dataset, with the goal of better understanding the effect of glints off horizontally oriented ice crystals on EPIC operational cloud products.

The outline of this article is as follows. Section II describes the dataset and then Section III examines statistical behaviors indicating whether the observed glints come from ice clouds or from the underlying water surface. Next, Section IV explores the impact of glints on the EPIC operational cloud products: cloud mask, cloud optical thickness (COT), and cloud altitude. Finally, Section V provides a brief summary and a few concluding remarks.

II. Datasets

This article presents a statistical analysis that considers all 5377 EPIC images taken during 2017. This dataset size was chosen so the analysis can consider an entire annual cycle for cloud and glint observation conditions. Because our interest lies in glints off ice clouds, we minimize the impact of glints off water surfaces by limiting the study to roughly 30% of images, in which the specular spot is over land. (The presence of land at the specular spot plus the availability

of Level 2 EPIC cloud and sun glint product files were the only data selection criteria; we used all 1656 images that satisfied them. We note that each image contained more than a dozen pixels in each category used in our statistical analysis.) We determine the surface cover type using the MODIS Land Cover Climate Modeling Grid (MCD12C1) product provided for the year 2017 [38]. First, we check whether a pixel is over water or land according to the parameter "Majority_Land_Cover_Type_1." For pixels over land, we also consider the parameter "Land_Cover_Type_1_Percent," which tells what fraction of the surface is covered by water. Unless noted otherwise, we only use data from pixels where the water cover is less than 1%. We note that the MCD12C1 product has a 0.05° latitude–longitude resolution which—in the tropical regions where EPIC can observe sun glint—corresponds to a roughly 5-km resolution. Therefore, we average the water coverage values over 5 × 5 grid cell arrays to cover the roughly (16 km)^2 fields-of-view of EPIC pixels. (While the sampling resolution near the center of EPIC images is about 8 km, the amount of data that needs to be transmitted to Earth from afar is reduced by a 2 × 2 averaging of all but the blue band (443 nm) images on the spacecraft. The images are then resampled to the original resolution on Earth.)

We examine the impact of cloud glints on EPIC reflectances and on the: 1) cloud mask; 2) COT; and 3) cloud height data provided in the EPIC cloud product [39], [40]. Because some glints are bright enough to cause detector saturation, we also use the pixelType flag included in the EPIC Level 1 data files. This flag identifies (via values >149) the pixels affected by saturation effects. We note that the reflectances reported for saturation-affected pixels are not always high: The spillage of signal along detector rows can create a series of low but identical reflectance values, as illustrated by the straight blue line in [4, Fig. 2(e)].

In addition, we also examine cloud height values provided in the EPIC composite cloud product [41]. This product is available for the 2015–2017 period and provides cloud properties based on geostationary and polar orbiting satellite data collocated with EPIC images. From the contents of this product, our analysis uses cloud height values that were calculated by a common algorithm applied to observations of the GOES-13 and -15, Meteosat-7 and -10, MTSAT-2, and Himawari-8 satellites. We use these values only if the time difference between EPIC and geostationary satellite observations is less than 15 min.

Finally, we note that we analyze our dataset using two statistical methods [the calculation of mean values and probability distribution functions (pdfs)] that provided valuable insights in countless studies of satellite datasets, including our earlier studies on clouds and sun glint (see [2], [3], [4], [5], [6], [7]). These techniques (used here to determine glint effects by comparing glint-prone and nearby glint-free regions) are now rather ubiquitous in science and in other spheres of life, even though the proposition of characterizing a dataset through the single number of its mean value (and ignoring all other information) initially met great resistance [42].

III. Glint Effects in the Presence of High Clouds and Water Surfaces

We begin by examining whether glint-caused reflectance increases are more intense when geostationary satellites report the presence of high clouds (likely to contain ice crystals). We use geostationary satellite data because they observe the regions of EPIC glints from a different, glint-less view direction, and hence can provide cloud information not affected by glint. As mentioned earlier, we rely on geostationary satellite data included in the EPIC composite cloud product.

To that end, Fig. 2 shows that glint-caused reflectance increases are larger for approximately 42% of EPIC observations where geostationary satellites indicate the presence of clouds above 3 km. The increases plotted in Fig. 2(a) are calculated as the difference between the mean reflectance of pixels with $\delta < 0.3°$ (pixels most affected by glints) and pixels with $1.5° < \delta < 2°$ (pixels outside most glints; see [2, Fig. 4]) where the glint angle δ is the angle between the EPIC view direction and the direction of specular reflection from a horizontal surface. Note also that the observation of stronger glints in the presence of high clouds is consistent with the results in [7], where oxygen absorption band data indicated that much of the signal of glint-affected pixels came from high altitudes.

The figure also shows that the reflectance increases vary considerably with wavelength regardless of whether high clouds are detected. As discussed in [7], these variations are due to two main factors: 1) Rayleigh scattering by the clear air above ice clouds weakens the glints at shorter wavelengths and 2) Gaseous absorption by ozone or oxygen weakens the glints at 317-, 325-, 688-, and 764-nm wavelengths.

Fig. 2 also shows that even though glint-induced reflectance increases are weaker when no high clouds are detected, they are still significant. Undoubtedly, some of these enhancements come from ice clouds that are so thin or small that either they cannot be detected, or their altitude cannot be accurately determined based on the radiances provided by geostationary satellites. Thus, glint observations can likely help with the sensitivity of ice cloud detection. At the same time, it is also possible that specular reflection from small water surfaces (that cover less than 1% of an EPIC pixel's area) also contribute to the glint-induced reflectance increases of Fig. 2. Therefore, we next explore the role of small water bodies.

Fig. 3 shows the way reflectance increases change as water covers an increasing fraction of EPIC pixels. Most importantly, the figure shows that the presence of small water bodies increases the glint signal substantially. At first, the effect grows quickly with increasing water coverage but then decreases. We note that, as shown in [7], the enhancements are only about 1/3 as strong for water pixels (with water cover >60%) than for land pixels. Our hypothesis is that glint effects decrease for larger water bodies because their surfaces tend to be wavier due to two reasons: 1) near-surface winds are stronger in the absence of nearby rough land surfaces that would slow the air movement (waves growing larger far from shore is often called fetching) and 2) large water bodies can feature waves that traveled from far-away, windier regions.

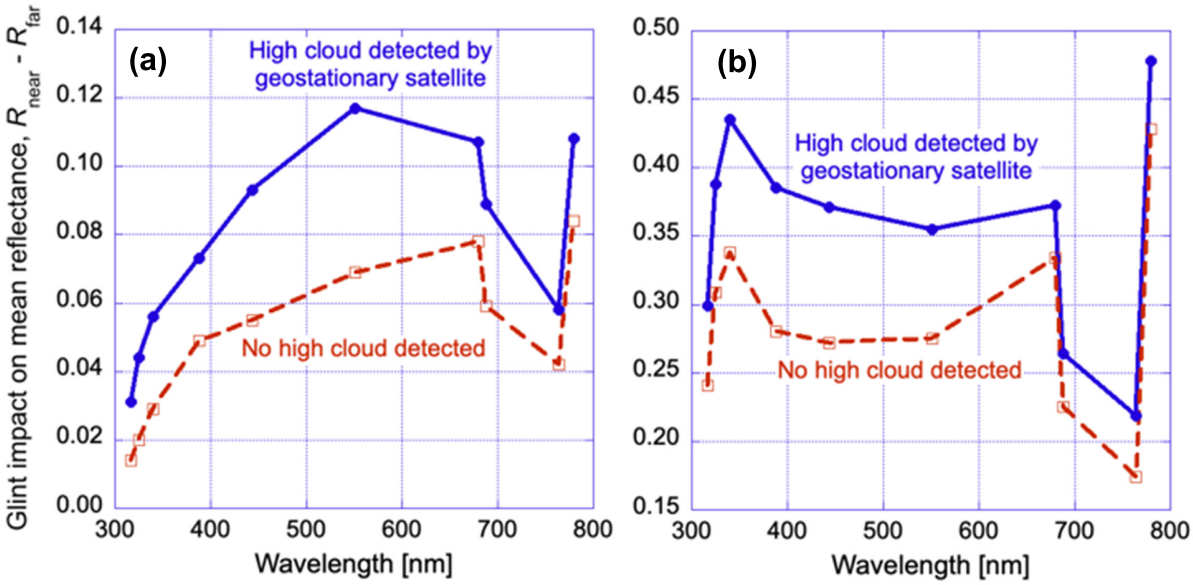

Fig. 2. Glint-induced reflectance increase is substantially stronger when geostationary satellites can confirm the presence of high clouds. (a) Glint impact is quantified via $R_{near} - R_{far}$, with R_{near} and R_{far} being the annual mean reflectance of pixels with glint angles δ in the 0°–0.3° and 1.5°–2° ranges, respectively. This difference quantifies the impact of glints off ice clouds on reflectance because these glints tend to affect only the areas near the specular spot, where the glint angle is less than 1.5°. Results are plotted separately for pixels where geostationary satellites did or did not detect clouds above 3 km. (b) Mean reflectance of pixels that are not affected by cloud glints as they are too far from the specular spot (and have 1.5°–2° glint angles). A comparison of the two plots reveals that, on average, glints increase reflectances by up to 33%. Both plots are based on land pixels in which water covers less than 1% of the EPIC field of view.

Roughness matters because the specular reflection from the variously tilted surfaces of waves will be spread over a wider range of directions. This spreading reduces reflectances for very small glint angles (e.g., $\delta < 0.3°$) while it increases reflectances in other directions, including those with 1.5°–2° glint angles (see [3])—thereby reducing the glint effects for pixels with extended bodies of water. We note, however, that the glint effects are always positive and substantial throughout Fig. 3.

Last, but not least, Fig. 3 shows that while for the driest land pixels, the enhancements are stronger when high clouds are detected, for land pixels with significant water cover the opposite is true (the enhancements are weaker when high clouds are detected). The reversal occurs when a large portion of the glint enhancements comes from the water surface. Although high clouds add their own glint enhancement signal, their main impact is to block some of the glint off the underlying water surface [35]. (In essence, clouds reduce the transmission of direct sunlight down to the surface and then back up to space.) This reversal is important because glint effects being stronger with high clouds than without them in the driest group of land pixels shows that the main source of glint from these pixels is indeed clouds: Had glints off water dominated, the glint signal would be weaker in the presence than in the absence of high clouds. Because Fig. 3 also shows that almost 94% of land pixels are in the driest category (with less than 1% water cover) and that almost 90% of the overall glint enhancements come from pixels in this category, we can conclude that this finding holds overall as well, which means that the main source of glints over land is ice clouds and not the surface.

IV. Glint Impacts on the EPIC Cloud Product

A. Cloud Mask

This section explores how glints off ice clouds affect the cloud mask provided in the EPIC cloud product. The current EPIC operational cloud detection algorithm [39] uses a single test (388-nm reflectance) for cloud detection over land. First, the contribution from Rayleigh scattering is removed from the observed reflectance, and then a pixel is deemed cloudy if the Rayleigh-removed 388-nm reflectance exceeds a certain threshold. A 388 nm is used because land surface reflectance is very low at this wavelength, and so large deviations from the reflectance expected for pure Rayleigh scattering can be confidently attributed to the presence of clouds.

The actual cloud detection uses multiple thresholds in order to classify each scene with an appropriate confidence level. The cloud mask classifies each pixel as either: 1) clear with high confidence; 2) clear with low confidence; 3) cloudy with low confidence; and 4) cloudy with high confidence. Just outside the areas where EPIC has a chance to observe glints off clouds (i.e., for $1.5° < \delta < 2°$), a 58% of land pixels are classified "cloudy with high confidence" and 4% are classified "cloudy with low confidence." Fig. 4 shows that glints can affect mean cloud fraction (CF), and that the impact depends on which EPIC band is affected by the glint.

The fairly large values of the solid black curve show that glints make the designation "cloudy with high confidence" significantly more frequent. This means that glints can help increase the sensitivity of cloud detection by enabling the detection of some thin or small ice clouds that we could not detect otherwise.

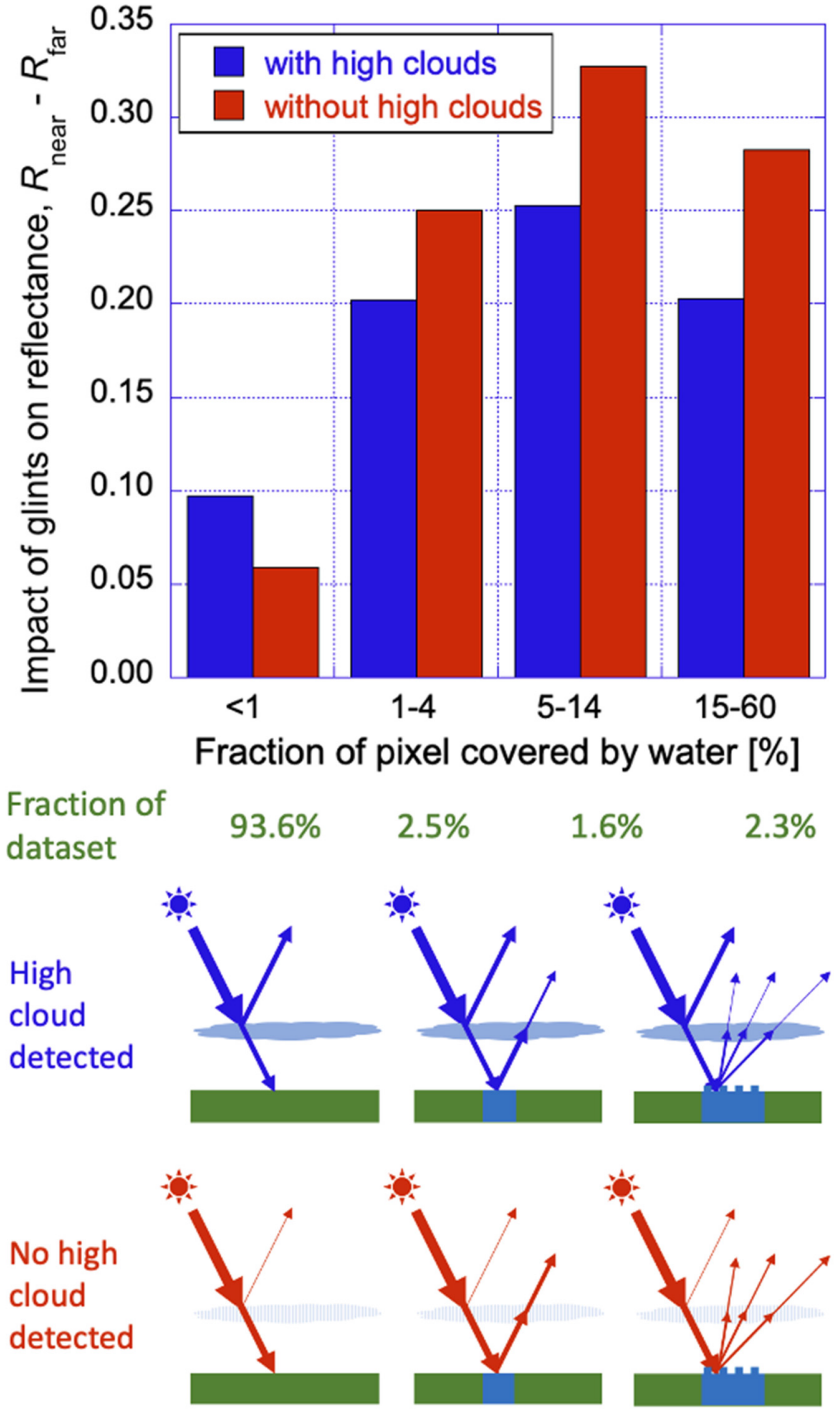

Fig. 3. Small water bodies (e.g., lakes) and high clouds strongly affect glints observations by EPIC. The glint impact (y-axis) is calculated as $R_{near} - R_{far}$, with R_{near} and R_{far} being the annual mean reflectance of pixels near and far from the specular spot (and having glint angles in the 0°–0.3° and 1.5°–2° ranges, respectively). Results are plotted separately for pixels where geostationary satellites did or did not detect clouds above 3 km, and for various degrees of water coverage. (Pixels with more than 60% water cover are not considered land pixels in the MODIS land cover map and hence are not the focus of our analysis.) To reduce random sampling noise, the reflectance enhancements are averaged for the 443, 551, 680, and 780 nm bands (that is, the four bands where Rayleigh scattering and gaseous absorption are least strong). The schematic graphs below illustrate glints in the presence (middle row) and absence (bottom row) of high cloud detection, for (left) dry land, (middle) small lakes, and (right). large wavy lakes.

It is worth noting that the solid curve peaks near the specular spot of the 388-nm band (S_{388}). This is because glint-induced CF increases peak right where glints have strong impact on 388-nm reflectances and increase them enough to surpass the cloud detection thresholds.

We also note that the solid curve drops as we move farther away from S_{388}. For example, the 388-nm reflectance test is expected to yield higher CF near S_{780} than near S_{764}. Since the time difference is smaller between 388- and 780-nm images than between the 388- and 764-nm images (Fig. 4), S_{388}

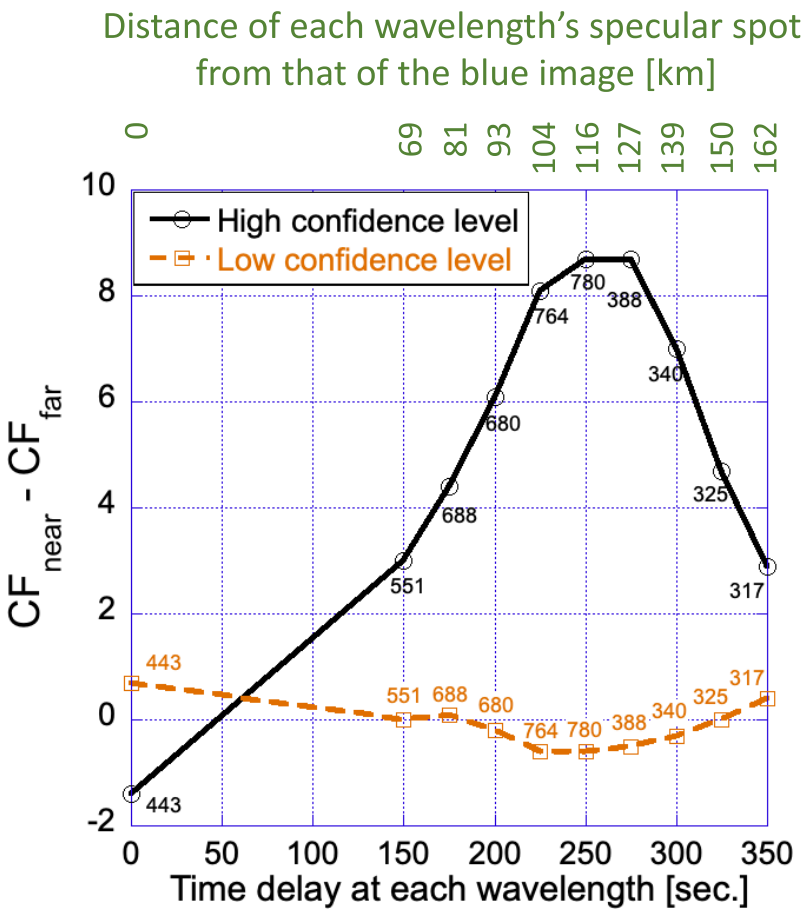

Fig. 4. Glints improve EPIC cloud detection by rendering it more sensitive to thin high clouds. The EPIC CF estimates are impacted mainly by glint-induced increases in the frequency of pixels deemed "cloudy with high confidence." This is quantified via $CF_{near} - CF_{far}$, with the subscripts "near" and "far" indicating pixels near and far from the specular spot (with 0°–0.3° and 1.5°–2° glint angles), respectively. As EPIC uses a filter wheel and takes images at each wavelength at slightly different times, Earth rotation causes different glint angles at each image. The labels next to the two line symbols identify the EPIC band whose specular spot and glint angles are used to calculate $CF_{near} - CF_{far}$. The time delay (and the corresponding shift in the specular spot's location, shown at the top) is chosen for the horizontal axis because images with similar time delays have similar glint geometries. For example, the 780- and 388-nm images being close in time implies that if a glint impacts the specular spot of the 780-nm image, it is likely that the 388-nm reflectance measured at the same location 25 s later is also affected by glint. In contrast, the same location has a very different geometry at the moment when the 443-nm image is taken 4 min earlier and is unlikely to have any glint effects in the 443-nm image. (The time gap is largest after the 443-nm image, which has a higher resolution and thus needs more time for data transmission to Earth.)

is closer to S_{780} than to S_{764}. Considering that a smaller distance from a specular spot implies a smaller glint angle, the glint angle in the 388-nm image is smaller and the 388-nm reflectance is larger (and is more likely to exceed the cloud detection threshold) at S_{780} than at S_{764} (thus leading to a higher CF near S_{780} than near S_{764}).

Finally, we note that the small values for the dashed orange line in Fig. 4 show that glints do not significantly affect the frequency of low-confidence cloud detections. This is because while glints shift some pixels from "clear" to "cloudy with low confidence," they also shift pixels from "cloudy with low confidence" to "cloudy with high confidence" or, in some cases, to "clear."

B. Cloud Optical Thickness

Over land, the EPIC operational data processing algorithm retrieves COT based on the 680-nm reflectance [39], [40]. Therefore, the effects of cloud glints on retrieved COT values can be evaluated by contrasting COTs for pixels near and far from the specular spot of the 680-nm image (again, glint angles are in the 0°–0.3° and 1.5–2 ranges in the near and far categories, respectively). Not surprisingly, glints enhancing 680-nm reflectances make the retrievals yield higher COT values. While the mean optical thickness is 13 far from the specular spot, it is 55 near the specular spot. To seek insights into this more than fourfold jump from 13 to 55, Fig. 5 examines the difference between the mean COT of the two glint angle ranges in individual EPIC images.

The pdf in Fig. 5 shows that in most images, the mean COT is similar near the specular spot and a bit farther away from it: While there is some natural variability due to the random arrangements of thinner and thicker clouds, the histogram has a strong peak around 0. At the same time, the pdf also features a long tail on the right side, which shows that in numerous scenes, the mean retrieved COT is much larger near the specular spot. Because no similar tail occurs on the left side, the right-side tail cannot be attributed to random variability but can be attributed to glints. This tail reveals that cloud glints can drastically increase retrieved COT values, sometimes by more than 100.

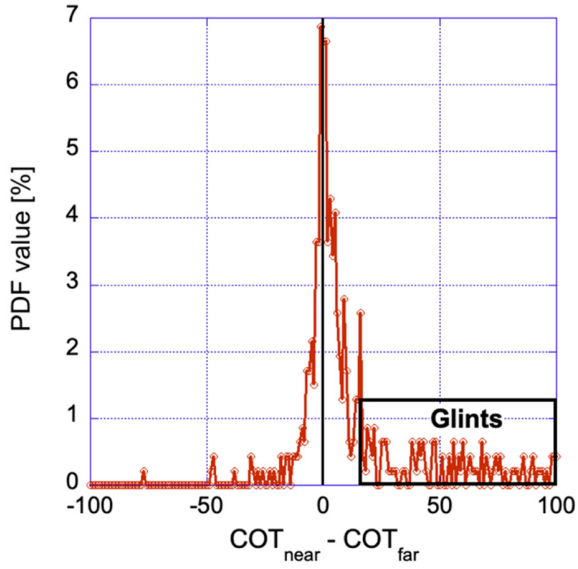

Fig. 5. Glints often cause large apparent jumps in cloud optical depths retrieved by EPIC. This figure shows the pdf of the difference between the mean COT values retrieved within each scene at areas near and far from the specular spot—that is, at areas where the sun-view geometry does or does not favor the observation of glints off ice crystals (due to glint angles being in the 0°–0.3° and 1.5°–2° range), respectively. The pdf is based on the 507 EPIC images that contain at least ten nonzero COT values in both the near and far categories.

Finally, we note that in some cases cloud glints are so bright that they cause detector saturation which, of course, makes COT retrievals unreliable. However, even if we only consider EPIC images that contain no detector saturation identified by the pixelType flag in the EPIC reflectance data files [43], the mean COT increases threefold from 13 to 39 as we approach the specular spot.

C. Cloud Height

The EPIC operational cloud product includes two separate cloud height values that are derived independently of one another: the effective cloud heights based on oxygen A-band or B-band data [39]. These height values can be expected to be somewhat different for two reasons: 1) oxygen absorption is weaker at the B-band than at the A-band, which means that the signal used for B-band height retrievals comes from lower altitudes deeper inside clouds and 2) variations in surface spectral properties and other conditions can have different impacts on A-band and B-band retrievals.

Despite these differences, the mean retrieved A-band and B-band cloud heights are very similar outside the potential cloud glint regions (for $1.5° < \delta < 2°$): 3213 and 3188 m for the A- and B-bands, respectively. Glints, however, have a drastically different impact on these heights. Near the specular spots (for $\delta < 0.3°$), the mean heights are 3392 and 4650 m for the A- and B-band, respectively. We note that the retrieved cloud heights are closely linked to some other parameters also reported in the EPIC cloud product, and so as retrieved cloud heights increase in glint areas, the retrieved values of cloud pressure and temperature decrease, and the estimated likelihood of ice cloud phase increases.

One reason why glints yield spuriously higher cloud altitudes is the saturation of 680- or 780-nm reflectances in bright glints. (Saturation is much less common for the 688- and 764-nm images that are also used in cloud height retrievals.) For example, the saturation of 680-nm reflectances can increase retrieved heights because it leads to a relatively smaller (detected) reflectance increase at 680 nm than at 688 nm, and so the B-band ratio $R_{688\ \mathrm{nm}}/R_{680\ \mathrm{nm}}$ (which is the primary parameter of the height retrievals) will increase. An example of saturation causing unexpectedly high retrieved cloud height values can be seen from Fig. 1.

The impact of saturation is further illustrated in Fig. 6. This figure is similar to Fig. 5, but it shows the histogram of the difference between the mean cloud heights (and not the mean COTs) of pixels near and far from the specular spot of the A-band or B-band images. Similar to Fig. 5, the lines in Fig. 6 also display a tail toward high values. This tail indicates that in some cases, glints greatly increase retrieved cloud height values, especially for the B-band retrievals. However, the tail gets substantially reduced if we consider only the images in which the pixelType flag does not indicate saturation. The reduction in the tail transfers to the retrieved mean heights: For example, while for B-band retrievals the mean height increases from 3188 to 4650 m near the specular spot if we consider all images, it increases from 3186 m to only 3821 m if we only consider unsaturated images. This reveals that more than half of the glint effects on the B-band retrievals can be attributed to detector saturation and perhaps other effects that are especially strong in glints that are bright enough to cause saturation.

One such effect is that the observed glints come from single scattering that occurs in the upper parts of clouds (glints caused by ice crystals located deeper in clouds are washed out by multiple scattering in the higher parts of clouds), whereas much of the non-glint reflection comes from multiple scattering at lower altitudes inside clouds (see [44]). Thus, the shorter path length for glint photons (than for photons of non-glint cloud reflection) will make glints increase the overall oxygen A- or B-band ratios and the altitude values retrieved from these ratios. Because the nonglint reflection comes from lower altitudes at the less absorbing B-band than at the more absorbing A-band, glints from the cloud top increase retrieved altitudes more for the B-band than for the A-band.

Another effect contributing to the right-side tail being stronger in Fig. 6(b) than in Fig. 6(a) is that the reflectivity of vegetated surfaces is higher around the A-band than the B-band. This matters because glints increase cloud contribution to reflectance without changing the surface contribution; hence the stronger surface contribution in the A-band implies that the relative change in the overall average photon path length (and retrieved altitude) is smaller in the A-band than in the B-band.

Yet another effect is that the absorbing and non-absorbing images are taken roughly 25 s apart and the Earth's rotation slightly changes the glint geometry during this time. As a result, glints can increase reflectances slightly more in one or the other channel and this can change the retrieved altitude values. For example, in areas where the difference in observation time leads to a smaller glint angle (and hence a stronger glint)

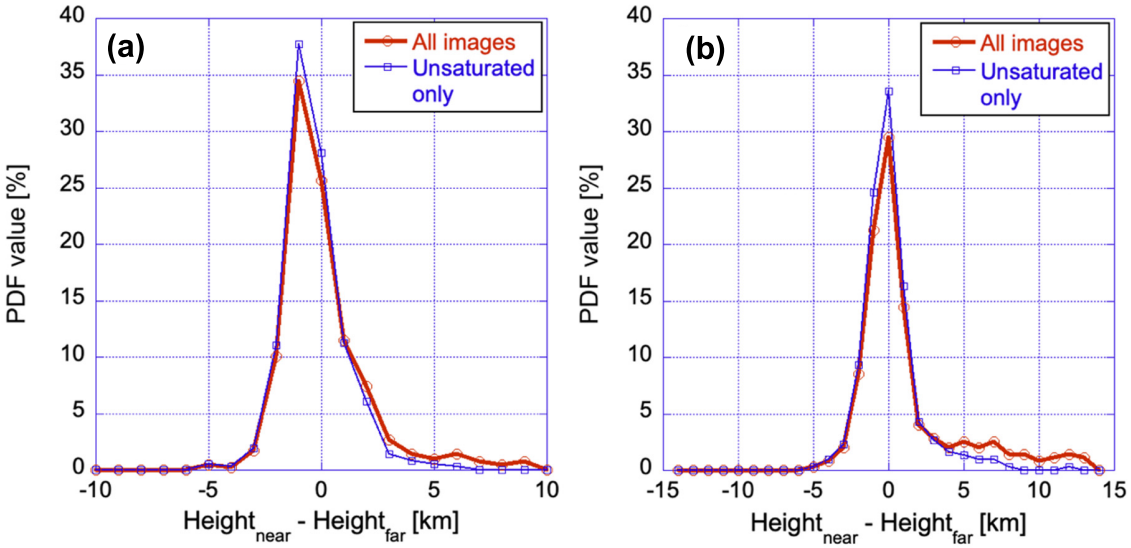

Fig. 6. Glints often cause large spurious jumps in retrieved cloud heights, with many coming from glint-induced detector saturation. pdfs of the difference in EPIC-retrieved cloud heights between near and far pixels (potentially affected and unaffected by glint, with glint angles in the 0°–0.3° and 1.5°–2° ranges, respectively). (a) Cloud heights retrieved using oxygen A-band data. (b) Cloud heights retrieved using oxygen B-band data. (Left and right) Calculated using glint angles for the oxygen A- and B-bands (764 and 688 nm), respectively. The PDFs are based on over 360 EPIC images that contain at least ten nonzero cloud height values in both the near and far categories.

for the 780-nm image than for the 764-nm image, this can reduce the A-band ratio and contribute to the negative height differences in Fig. 6(a). However, because of the nonlinearity of the link between oxygen absorption and altitude (see [39, Fig. 3(a)]), the differences between the glint enhancements at absorbing and nonabsorbing wavelengths change the retrieved altitude values more when the change is toward higher (and not lower) altitudes—which contributes to the skewed behaviors in Fig. 6.

Finally, we point out that while in Fig. 5, the curve is fairly symmetric around 0 (except for the long tail to the right), the peaks in Fig. 6(a) display a slight but clear leftward shift. This is likely caused by the signal from the (low altitude) ground, which is especially strong around the A-band due to the high near-infrared reflectivity of vegetated surfaces. This ground signal may reach EPIC through thin clouds or through gaps between clouds and is not accounted for in the height retrieval algorithm when bright glints are present. This is because bright glints make the algorithm think that the area is fully covered by (opaque) clouds and so the entire signal comes from the clouds that block any signal from the surface. This becomes a concern in partly cloudy pixels (that appear overcast to the algorithm only because of the bright glint), where a significant portion of the observed reflectances come from the ground. As the photons coming from the ground travel a long pathlength through the atmosphere, oxygen absorption along the way reduces the pixel's observed A-band and B-band ratios. Since the algorithm does not expect this, the reduction leads to an underestimation of cloud altitude.

V. Summary

This article examined sun glints observed by the EPIC instrument over land areas, with the goal of better understanding both the source of these glints and the glints' impact on the operational cloud products provided by EPIC: CF, cloud optical thickness, and cloud height. With this goal in mind, the article described a statistical analysis of all 5377 images EPIC provided during 2017, of which 1656 had landed at the specular spot ideal for glint observations. Analyzing a yearlong dataset led to relatively small statistical error margins and allowed us to clearly identify the key behaviors.

First, the analysis revealed that in the great majority of land pixels that have minimal (if any) subpixel water cover, glints are significantly stronger when collocated geostationary satellites detect high clouds. This trend, however, is reversed in pixels with significant water cover (around lakes, rivers, and coastlines), where clouds can block glints from water surfaces. The combination of these findings suggests that over land, the main source of glints is indeed specular reflection from ice clouds. Finally, the significant glint-caused increases of reflectance for water-free pixels suggest that if satellite data can identify the altitude of glint signals (for example, through observations at oxygen absorption bands), glints may help enhance the sensitivity of cloud detection in cases of thin ice clouds. Future investigations of the cases where glint is observed even though geostationary satellites do not indicate high clouds could provide further insights into these glints and their possible use in cloud detection.

In examining the impact of glints on operational EPIC cloud products, the analysis found that retrieved CF increases by 0.09 in water-free land areas where the sun-view geometry is favorable to observing sun glint. This increase is due to the specular reflection of glints enhancing 388-nm reflectances past the cloud detection thresholds.

Glints were also found to drastically and spuriously increase retrieved cloud optical thicknesses: The mean retrieved COT of water-free land areas was four times larger (≈55) if sun-view geometry was favorable to observe glints than in nearby areas

with glint-avoiding view geometry (≈13). It was also found that in individual EPIC images, glint-related COT enhancements can exceed 100. Some of the largest enhancements occurred in very bright glints that caused detector saturation, but even if images with saturation were excluded, glints increased mean COT threefold (from 13 to 39) in areas with glint-favoring observation geometry.

Finally, the analysis showed that glints can greatly increase or slightly decrease retrieved cloud heights. The large increases were tentatively attributed to several effects, including glints coming from higher altitudes than non-glint cloud reflection, and Earth rotation causing different glint geometry for images taken at absorbing and nonabsorbing wavelengths. The largest increases, however, could be linked to glints causing detector saturation mainly at nonabsorbing wavelengths (680 and 780 nm). This saturation caps, for example, the 680-nm reflectance values reported, which leads to increases in the ratio of reflectances at the 688- and 680-nm bands. Height retrievals using oxygen B-band data then interpret this increase as a sign of high cloud altitude. On the other hand, some glints were found to cause moderate underestimations of cloud altitude, especially in retrievals based on oxygen A-band data. This underestimation occurs when bright glints off ice crystals in an area covered by broken or thin ice clouds make retrievals think that all the signal comes from an overcast thick cloud layer. The part of the signal that in reality comes from a highly reflective underlying surface is misinterpreted as a sign of lower cloud altitude.

The most important limitation of this study is that it provides information only about tropical regions and only around local noon, as the EPIC observational geometry does not allow glint observations at higher latitudes or in early mornings and late afternoons. In future studies, data from polar orbiting and geostationary satellites may provide further insights into glint effects at higher latitudes and at different local times, respectively. Future glint studies may also take advantage of additional capabilities of planned satellite missions such as PACE, which will provide multi-angle polarization observations [45]. Finally, future analyses may also improve upon the present study by examining datasets that cover longer periods than the one year considered here; this will reduce the margins of errors due to the finite sample size and interannual variability.

Overall, the results show that glints over land come mainly from ice clouds and that they greatly affect operational cloud products. Fortunately, the area covered by glints off ice clouds is limited to areas where the EPIC glint angle is less than about 1.5°, and so the impact of glints on global cloud statistics is not a major concern. However, it is important to be aware and consider the possible effects of glints in case studies or in studies that examine tropical regions around noon (where EPIC can see glints), for example, in examining cloud daily cycles or in investigating deep convective clouds (with whom glints may be confused as both are very bright and occur at high altitudes). The glint impacts may be especially significant in considering higher-order moments or histograms of cloud properties. It is important to note that cloud glint effects impact not only EPIC but also other satellites that use similar methodologies for cloud characterization. As a result, we believe that it is important to be mindful of and to identify glints off ice clouds (for example, using the EPIC sun glint product [2]) and to understand their effects. At the same time, we should also keep in mind that, as mentioned in the introduction, glint observations provide helpful information about the presence of horizontally oriented ice crystals and may help reducing uncertainties in a variety of applications ranging from radiative calculations and microwave retrievals of cloud ice water content to calculations of ice crystal fall speed and cloud lifetime or constraining cloud conditions.

REFERENCES

[1] A. Marshak et al., "Earth observations from DSCOVR EPIC instrument," *Bull. Amer. Meteorol. Soc.*, vol. 99, no. 9, pp. 1829–1850, Sep. 2018, doi: 10.1175/bams-d-17-0223.1.

[2] T. Várnai, A. Marshak, and A. Kostinski, "Operational detection of sun glints in DSCOVR EPIC images," *Frontiers Remote Sens.*, vol. 2, Nov. 2021, Art. no. 777806, doi: 10.3389/frsen.2021.777806.

[3] T. Várnai, A. B. Kostinski, and A. Marshak, "Deep space observations of sun glints from marine ice clouds," *IEEE Geosci. Remote Sens. Lett.*, vol. 17, no. 5, pp. 735–739, May 2020, doi: 10.1109/LGRS.2019.2930866.

[4] A. Kostinski, A. Marshak, and T. Várnai, "Deep space observations of terrestrial glitter," *Earth Space Sci.*, vol. 8, no. 2, Feb. 2021, Art. no. e2020EA001521, doi: 10.1029/2020ea001521.

[5] A. Marshak, T. Várnai, and A. Kostinski, "Terrestrial glint seen from deep space: Oriented ice crystals detected from the Lagrangian point," *Geophys. Res. Lett.*, vol. 44, no. 10, pp. 5197–5202, May 2017, doi: 10.1002/2017gl073248.

[6] J. Li et al., "Study of terrestrial glints based on DSCOVR observations," *Earth Space Sci.*, vol. 6, no. 1, pp. 166–173, Jan. 2019, doi: 10.1029/2018ea000509.

[7] T. Várnai, A. Marshak, and A. B. Kostinski, "Deep space observations of cloud glints: Spectral and seasonal dependence," *IEEE Geosci. Remote Sens. Lett.*, vol. 19, pp. 1–5, 2022, doi: 10.1109/LGRS.2020.3040144.

[8] F.-M. Bréon and B. Dubrulle, "Horizontally oriented plates in clouds," *J. Atmos. Sci.*, vol. 61, no. 23, pp. 2888–2898, Dec. 2004, doi: 10.1175/jas-3309.1.

[9] H. Chepfer, G. Brogniez, P. Goloub, F. M. Bréon, and P. H. Flamant, "Observations of horizontally oriented ice crystals in cirrus clouds with POLDER-1/ADEOS-1," *J. Quant. Spectrosc. Radiat. Transf.*, vol. 63, nos. 2–6, pp. 521–543, Sep. 1999, doi: 10.1016/s0022-4073(99)00036-9.

[10] V. Noel and H. Chepfer, "Study of ice crystal orientation in cirrus clouds based on satellite polarized radiance measurements," *J. Atmos. Sci.*, vol. 61, pp. 2073–2081, 1175, doi: 10.1175/1520-0469(2004)061<2073:SOICOI>2.0.CO;2.

[11] V. Noel and H. Chepfer, "A global view of horizontally oriented crystals in ice clouds from cloud-aerosol LiDAR and infrared pathfinder satellite observation (CALIPSO)," *J. Geophys. Res., Atmos.*, vol. 115, no. D4, Feb. 2010, Art. no. D00H23, doi: 10.1029/2009jd012365.

[12] M. Kikuchi, H. Okamoto, and K. Sato, "A climatological view of horizontal ice plates in clouds: Findings from nadir and off-nadir CALIPSO observations," *J. Geophys. Res., Atmos.*, vol. 126, no. 9, May 2021, Art. no. e2020JD033562, doi: 10.1029/2020jd033562.

[13] Y. J. Kaufman, J. V. Martins, L. A. Remer, M. R. Schoeberl, and M. A. Yamasoe, "Satellite retrieval of aerosol absorption over the oceans using sunglint," *Geophys. Res. Lett.*, vol. 29, no. 19, pp. 1–34, Oct. 2002, doi: 10.1029/2002gl015403.

[14] M. Ottaviani, K. Knobelspiesse, B. Cairns, and M. Mishchenko, "Information content of aerosol retrievals in the sunglint region," *Geophys. Res. Lett.*, vol. 40, no. 3, pp. 631–634, Feb. 2013, doi: 10.1002/grl.50148.

[15] K. Knobelspiesse et al., "Analysis of simultaneous aerosol and ocean glint retrieval using multi-angle observations," *Atmos. Meas. Techn.*, vol. 14, no. 5, pp. 3233–3252, May 2021, doi: 10.5194/amt-14-3233-2021.

[16] J. I. Katz, "Subsuns and low Reynolds number flow," *J. Atmos. Sci.*, vol. 55, pp. 3358–3362, 1998, doi: 10.1175/1520-0469(1998)055<3358:SALRNF>2.0.CO;2.

[17] D. K. Lynch, S. D. Gedzelman, and A. B. Fraser, "Subsuns, Bottlinger's rings, and elliptical halos," *Appl. Opt.*, vol. 33, no. 21, p. 4580, 1994, doi: 10.1364/ao.33.004580.

[18] D. K. Lynch and W. Livingston, *Color and Light in Nature*. Cambridge, U.K.: Cambridge Univ. Press, 2001.

[19] G. P. Koönnen, "Rainbows, halos, coronas and glories: Beautiful sources of information," *Bull. Amer. Meteorol. Soc.*, vol. 98, pp. 485–494, 2017, doi: 10.1175/BAMS-D-16-0014.1.

[20] Y. Takano and K.-N. Liou, "Solar radiative transfer in cirrus clouds. Part II: Theory and computation of multiple scattering in an anisotropic medium," *J. Atmos. Sci.*, vol. 46, no. 1, pp. 20–36, Jan. 1989.

[21] R. A. Stillwell, R. R. Neely, J. P. Thayer, V. P. Walden, M. D. Shupe, and N. B. Miller, "Radiative influence of horizontally oriented ice crystals over summit, Greenland," *J. Geophys. Res., Atmos.*, vol. 124, no. 22, pp. 12141–12156, Nov. 2019.

[22] J. Gong and D. L. Wu, "Microphysical properties of frozen particles inferred from global precipitation measurement (GPM) microwave imager (GMI) polarimetric measurements," *Atmos. Chem. Phys.*, vol. 17, no. 4, pp. 2741–2757, Feb. 2017.

[23] X. Zeng, J. Gong, X. Li, and D. L. Wu, "Modeling the radiative effect on microphysics in cirrus clouds against satellite observations," *J. Geophys. Res., Atmos.*, vol. 126, no. 4, Feb. 2021, Art. no. e2020JD033923, doi: 10.1029/2020jd033923.

[24] A. J. Heymsfield and J. Iaquinta, "Cirrus crystal terminal velocities," *J. Atmos. Sci.*, vol. 57, pp. 916–938, 2000, doi: 10.1175/1520-0469(2000)057<0916:CCTV>2.0.CO;2.

[25] C. D. Westbrook, "The fall speeds of sub-100 μm ice crystals," *Quart. J. Roy. Meteorol. Soc.*, vol. 134, no. 634, pp. 1243–1251, Jul. 2008, doi: 10.1002/qj.290.

[26] P. Yang, S. Hioki, M. Saito, C.-P. Kuo, B. Baum, and K.-N. Liou, "A review of ice cloud optical property models for passive satellite remote sensing," *Atmosphere*, vol. 9, no. 12, p. 499, Dec. 2018, doi: 10.3390/atmos9120499.

[27] M. Saito and P. Yang, "Oriented ice crystals: A single-scattering property database for applications to LiDAR and optical phenomenon simulations," *J. Atmos. Sci.*, vol. 76, no. 9, pp. 2635–2652, Sep. 2019, doi: 10.1175/jas-d-19-0031.1.

[28] I. Veselovskii et al., "Spectral dependence of backscattering coefficient of mixed phase clouds over West Africa measured with two-wavelength Raman polarization LiDAR: Features attributed to ice-crystals corner reflection," *J. Quant. Spectrosc. Radiat. Transf.*, vol. 202, pp. 74–80, Nov. 2017, doi: 10.1016/j.jqsrt.2017.07.028.

[29] A. Borovoi, A. Konoshonkin, N. Kustova, and H. Okamoto, "Backscattering Mueller matrix for quasi-horizontally oriented ice plates of cirrus clouds: Application to CALIPSO signals," *Opt. Exp.*, vol. 20, no. 27, pp. 28222–28233, 2012, doi: 10.1364/oe.20.028222.

[30] A. G. Borovoi, A. V. Konoshonkin, N. V. Kustova, and I. A. Veselovskii, "Contribution of corner reflections from oriented ice crystals to backscattering and depolarization characteristics for off-zenith LiDAR profiling," *J. Quant. Spectrosc. Radiat. Transf.*, vol. 212, pp. 88–96, Jun. 2018, doi: 10.1016/j.jqsrt.2018.03.022.

[31] Y. He, F. Liu, Z. Yin, Y. Zhang, Y. Zhan, and F. Yi, "Horizontally oriented ice crystals observed by the synergy of zenith- and slant-pointed polarization LiDAR over Wuhan (30.5 °N, 114.4 °E), China," *J. Quant. Spectrosc. Radiat. Transf.*, vol. 268, Jul. 2021, Art. no. 107626, doi: 10.1016/j.jqsrt.2021.107626.

[32] M. Wang and S. W. Bailey, "Correction of sun glint contamination on the SeaWiFS ocean and atmosphere products," *Appl. Opt.*, vol. 40, pp. 4790–4798, 2001, doi: 10.1364/AO.40.004790.

[33] L. A. Remer et al., "The MODIS aerosol algorithm, products, and validation," *J. Atmos. Sci.*, vol. 62, pp. 947–973, Apr. 2005, doi: 10.1175/JAS3385.1.

[34] R. C. Levy et al., "The Collection 6 MODIS aerosol products over land and ocean," *Atmos. Meas. Techn.*, vol. 6, no. 11, pp. 2989–3034, Nov. 2013, doi: 10.5194/amt-6-2989-2013.

[35] Y. Zhou, Y. Yang, P.-W. Zhai, and M. Gao, "Cloud detection over sunglint regions with observations from the Earth polychromatic imaging camera," *Frontiers Remote Sens.*, vol. 2, Jul. 2021, Art. no. 690010, doi: 10.3389/frsen.2021.690010.

[36] G. Tana et al., "Retrieval of cloud microphysical properties from Himawari-8/AHI infrared channels and its application in surface shortwave downward radiation estimation in the sun glint region," *Remote Sens. Environ.*, vol. 290, May 2023, Art. no. 113548, doi: 10.1016/j.rse.2023.113548.

[37] H. Shang et al., "A hybrid cloud detection and cloud phase classification algorithm using classic threshold-based tests and extra randomized tree model," *Remote Sens. Environ.*, vol. 302, Mar. 2024, Art. no. 113957, doi: 10.1016/j.rse.2023.113957.

[38] M. Friedl and D. Sulla-Menashe, "MODIS/Terra+Aqua land cover type yearly L3 global 0.05Deg CMG V006," NASA EOSDIS Land Processes DAAC, Washington, DC, USA, Tech. Rep. MCD12C1, 2016, doi: 10.5067/MODIS/MCD12C1.006.

[39] Y. Yang et al., "Cloud products from the Earth polychromatic imaging camera (EPIC): Algorithms and initial evaluation," *Atmos. Meas. Techn.*, vol. 12, no. 3, pp. 2019–2031, Mar. 2019, doi: 10.5194/amt-12-2019-2019.

[40] K. Meyer, Y. Yang, and S. Platnick, "Uncertainties in cloud phase and optical thickness retrievals from the Earth polychromatic imaging camera (EPIC)," *Atmos. Meas. Techn.*, vol. 9, no. 4, pp. 1785–1797, Apr. 2016, doi: 10.5194/amt-9-1785-2016.

[41] *EPIC-view Satellite Composites for DSCOVR, Version 1*, document C1576365803-LARC_ASDC, NASA Langley Atmos. Sci. Data Center DAAC, 2015, doi: 10.5067/EPIC/DSCOVR/L2_COMPOSITE_01.

[42] S. M. Stigler, *The Seven Pillars of Statistical Wisdom*. Cambridge, MA, USA: Harvard Univ. Press, 2016.

[43] A. Cede et al., "Raw EPIC data calibration," *Frontiers Remote Sens.*, vol. 2, Jul. 2021, Art. no. 702275, doi: 10.3389/frsen.2021.702275.

[44] S. Platnick, "Vertical photon transport in cloud remote sensing problems," *J. Geophys. Res., Atmos.*, vol. 105, no. D18, pp. 22919–22935, Sep. 2000, doi: 10.1029/2000jd900333.

[45] P. J. Werdell et al., "The plankton, aerosol, cloud, ocean ecosystem mission: Status, science, advances," *Bull. Amer. Meteorolog. Soc.*, vol. 100, no. 9, pp. 1775–1794, Sep. 2019, doi: 10.1175/BAMS-D-18-0056.1.

Tamás Várnai received the M.S. degree equivalent diploma in meteorology from Eötvös Loràind University, Budapest, Hungary, in 1989, and the Ph.D. degree in atmospheric and oceanic sciences from McGill University, Montreal, QC, Canada, in 1996.

From 1997 to 1999, he was a Post-Doctoral Fellow with the University of Arizona, Tucson, AZ, USA, and from 1989 to 1991, he was a Research Scientist with Hungarian Meteorological Service. He is currently a Research Associate Professor with the University of Maryland, Baltimore County, Baltimore, MD, USA, and also with the NASA's Goddard Space Flight Center and Goddard Earth Sciences Technology and Research (GESTAR) II, Greenbelt, MD, USA. His research interests focus on 3-D radiative processes and on satellite remote sensing of clouds and atmospheric aerosols.

Alexander Marshak received the M.S. degree in applied mathematics from Tartu University, Tartu, Estonia, in 1978, and the Ph.D. degree in numerical analysis from the Academy of Sciences, Novosibirsk, Russia, in 1983.

In 1978, he joined the Institute of Astrophysics and Atmospheric Physics, Tartu, where he worked for 11 years. In 1991, he joined the NASA Goddard Space Flight Center (GSFC), Greenbelt, MD, USA, first working for Science Systems and Applications Inc. (SSAI); then Joint Center for Earth Systems Technology (JCET), University of Maryland, Baltimore County (UMBC), Baltimore, MD, USA; and finally, NASA/GSFC, where he has been since January 2003. He conducts research on remote sensing of clouds, aerosols, and blowing snow, on cloud–aerosol interaction, and on many aspects of atmospheric radiative transfer.

Dr. Marshak received an Alexander von Humboldt Fellowship and worked for two years with Göttingen University, Göttingen, Germany, in 1989. He is the Deputy Project Scientist for the Deep Space Climate Observatory (DSCOVR) Satellite Mission, and a member of the CALIPSO and MODIS Science Teams, and the International Radiation Commission.

Alexander (Alex) B. Kostinski has been with Michigan Technological University (MTU), Houghton, MI, USA, since 1989, where he is currently a Professor of physics. He was funded by the National Science Foundation for over 30 years as a sole PI and his publications have ranged broadly from optics, fluid mechanics, and astrophysics to radar meteorology, atmospheric science, and statistical signal analysis. He has taught most of the graduate and senior undergraduate courses offered by the Physics Department, MTU. He is currently contributing to the APAR Program. He is also currently an Affiliate Scientist with the National Center for Atmospheric Research.

Yuekui Yang received the Ph.D. degree in atmospheric sciences from the University of Illinois at Urbana–Champaign, Champaign, IL, USA, in 2007.

He worked as a Research Scientist and the Group Leader at the Universities Space Research Association, where his affiliation began in 2011. From 2007 to 2011, he was associated with the University of Maryland, Baltimore County, Baltimore, MD, USA. He has been a Research Physical Scientist with the NASA Goddard Space Flight Center, Greenbelt, MD, USA, since 2016. His research interests include satellite cloud property analysis, studies of cloud and blowing snow over polar ice sheets, polar radiation budget, and polar boundary layer properties.

Yaping Zhou received the B.S. degree in climatology from Nanjing University, Nanjing, China, in 1988, the M.S. degree in climate dynamics from the Institute of Atmospheric Physics, Chinese Academy of Sciences, Beijing, China, in 1991, and the M.S. degree in computer science and Ph.D. degree in atmospheric science from Stony Brook University, Stony Brook, NY, USA, in 1999.

She is currently a Senior Research Scientist at the University of Maryland, Baltimore County, Baltimore, MD, USA, affiliated with the NASA's Goddard Space Flight Center, Greenbelt, MD, USA. With prior experience at the NASA Langley Research Center and the Climate Prediction Center of NCEP/NOAA, her interests include climate trends, large-scale tropical hydrological cycles, atmospheric convection, extreme precipitation, numerical model validation, and remote sensing. She has contributed to algorithm development for multiple operational remote sensing systems employed by NASA, including those utilized by CERES, MODIS, VIIRS, and Deep Space Climate Observatory (DSCOVR) EPIC instruments. Currently, her focus lies on advancing physical retrieval algorithms for future hyperspectral microwave instruments.